Inorg. Chem. **2004**, *43*, 3561–3572

Structure and Dynamics of Dinuclear Zirconium(IV) Complexes

Weiqing Zhong,[†,‡] John A. Parkinson,[§,‡] Simon Parsons,[‡] Iain D. H. Oswald,[‡] Robert A. Coxall,[‡] and Peter J. Sadler*[,‡]

School of Pharmacy, Second Military Medical University, Shanghai 200433, P. R. China, and School of Chemistry, University of Edinburgh, King's Buildings, West Mains Road, Edinburgh EH9 3JJ, U.K.

Received January 16, 2004

We have determined by X-ray crystallography the structures of three dinuclear zirconium(IV) complexes containing the heptadentate ligand dhpta (where H_5dhpta = 1,3-diamino-2-propanol-*N,N,N′,N′*-tetraacetic acid, **1**) and different countercations: $K_2[Zr_2(dhpta)_2]\cdot 5H_2O$ (**2**·$5H_2O$), $Na_2[Zr_2(dhpta)_2]\cdot 7H_2O\cdot C_2H_5OH$ (**3**·$7H_2O$·C_2H_5OH), and $Cs_2[Zr_2(dhpta)_2]\cdot H_5O_2\cdot Cl\cdot 4H_2O$ (**4**·H_5O_2·Cl·$4H_2O$). In the K(I) complex **2**, crystallized from water, the two Zr(IV) ions are 3.5973(4) Å apart and bridged via two alkoxo groups (average Zr–O 2.165 Å). Each Zr(IV) is eight-coordinate and also bound to two N atoms (average Zr–N 2.448 Å), and four carboxylate O atoms (average Zr–O 2.148 Å). The two dhpta ligands in the dinuclear unit have different conformations. One face of the complex contains an array of 14 oxygen atoms and interacts strongly with the two K(I) ions, one of which is 6-coordinate, the other 8-coordinate, which are 3.922(4) Å apart and bridged by a carboxylate O and by two water molecules. The structures of the dinuclear anion $[Zr_2(dhpta)_2]^{2-}$ in the Na(I) complex **3** and in the Cs(I) complex **4** are essentially identical to that found in complex **2**, although the alkali metal ions coordinate differently to the oxygen-rich face. All Zr(IV) ions have a distorted triangulated dodecahedral geometry. Although the crystal structure of complex **2** does not indicate the presence of acidic protons, in **4** an $[H_5O_2]^+$ unit is strongly H-bonded to an oxygen atom of a coordinated carboxylate group. 1D and 2D ^{1}H and ^{13}C NMR spectroscopic and potentiometric studies reveal two deprotonations with pK_a values of 9.0 and 10.0. At low pH, two carboxylate groups appear to undergo protonation accompanied by chelate ring-opening, and the complex exhibits dynamic fluxional behavior in which the two magnetically nonequivalent dhpta ligands exchange at a rate of 11 s^{-1} at pH 3.30, 298 K, as determined from 2D EXSY NMR studies. Ligand interchange is not observed at high pH (>11). The same crystals of complex **2** were obtained from solutions at pH 3 or 12. The dynamic configurational change is therefore mediated by the aqueous solvent.

Introduction

We are interested in the biological and medicinal chemistry of zirconium and the possibility of designing Zr compounds as therapeutic agents. Although Zr has no known natural biological role, it is reported to be present in the body at levels similar to the essential elements Co and Mo.[1−4] Current uses of Zr and Zr compounds in medicine center on artificial joints for limb and hip replacements,[5] antiperspirants,[6,7] and adjuvants for antibody production.[8] Attempts to design Zr complexes as anticancer agents have so far been unsuccessful; although Cp_2TiCl_2 exhibits anticancer activity, Cp_2ZrCl_2 is inactive.[9] Zr(IV) binds strongly to the Fe(III) sites of both

* To whom correspondence should be addressed. E-mail: P.J.Sadler@ed.ac.uk. Fax: +44 131 650 6453.
† Second Military Medical University.
‡ University of Edinburgh.
§ Current address: Department of Pure and Applied Chemistry, University of Strathclyde, Glasgow G1 1XL, U.K.

(1) Underwood, E. J. In *Trace elements in human and animal nutrition*; Academic Press: London, 1976; pp 452−453.
(2) Ghosh, S.; Sharma, A.; Talukder, G. *Biol. Trace Elem. Res.* **1992**, *35*, 247−271.
(3) Lin, L. Q.; Wen, H. F. *Zhonghua Yufang Yixue Zazhi* **1988**, *22*, 98−100.
(4) Koutzenogii, K. P.; Savchenko, T. I.; Chankina, O. V.; Kovalskaya, G. A.; Osipova, L. P.; Bgatov. A. V. *J. Trace Microprobe Techn.* **2003**, *21*, 311−325.
(5) (a) Goldsmith, A. A. J.; Dowson, D.; Isaac, G. H.; Lancaster, J. G. *Proc. Inst. Mech. Engrs.* **2000**, *H214*, 39−47. (b) Basle, M. F.; Bertrand, G.; Guyetant, S.; Chappard, D.; Lesourd, M. *J. Biomed. Mater. Res.* **1996**, *30*, 157−164.
(6) Montemarano, A. D.; Sau, P.; Johnson, F. B.; James, W. D. *J. Am. Acad. Dermatol.* **1997**, *37*, 496−498.
(7) Quatrale, R. P.; Coble, D. W.; Stoner, K. L.; Felger, C. B. *J. Soc. Cosmet. Chem.* **1981**, *32*, 195−221.
(8) Shima, S.; Morita, K.; Tachikawa, S.; Ito, T.; Kurita, H.; Yoshida, T.; Kato, Y.; Yamamoto, Y. *Br. J. Ind. Med.* **1987**, *44*, 633−637.

10.1021/ic049932k CCC: $27.50
Published on Web 05/12/2004

bacterial and human transferrins, and these proteins could play potential roles in the uptake and transport of Zr(IV) in the body and in microorganisms.[10]

The aqueous coordination chemistry of Zr(IV) is relatively unexplored. It is dominated by hydrolysis to give hydroxide-containing species, oxo-linked polymers, and subsequent precipitation even at low pH (3.5). For example, the tetramer $[Zr_4(OH)_8(H_2O)_{16}]^{8+}$ is the predominant species in both crystals and aqueous solutions of $ZrOCl_2 \cdot 8H_2O$.[11] The trimers $[Zr_3(OH)_4]^{8+}$ and $[Zr_3(OH)_5]^{7+}$ and monomer complexes $[Zr(OH)_h]^{(4-h)+}$ ($h = 1-5$) can also exist at low pH in solutions of low concentration.[12] The Zr(IV) ions are hydroxide-bridged in these cluster complexes and convert to oxo-linked precipitates when the pH is increased. Aminocarboxylate ligands bind strongly to Zr(IV), and complexes such as $[Zr(nta)_2]^{2-}$ and $[Zr(edta)X_2]^{2-}$ (nta = nitrilotriacetate, edta = ethylenediaminetetraacetate; $X = {}^1/_2CO_3^{2-}$, F^-, H_2O) have been reported,[13−15] some of which have been crystallized from aqueous solutions. There are few reported studies of the solution chemistry of these types of complexes.

In the present work, we have studied Zr(IV) binding to the aminocarboxylate ligand, 1,3-diamino-2-hydroxypropane-*N*,*N*,*N*′,*N*′-tetraacetic acid (H_5dhpta, **1**). Complexes of this ligand with Fe(III) and several other transition metals have been widely studied previously to gain insight into their chemical and magnetic properties as models for multinuclear metal centers in non-heme and other proteins.[16,17] We report here the synthesis and characterization of new dinuclear Zr(IV) complexes of **1** which have interesting acidic properties and undergo dynamic structural transitions in aqueous solution.

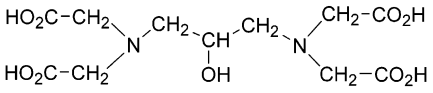

1 (H_5dhpta)

Experimental Section

Materials. H_5dhpta, Hepes, H_3nta, and Fe and Zr atomic absorption standard solutions were purchased from Aldrich, $NaH[^{13}C]O_3$ (> 99% enriched) was purchased from MSD isotopes, and $ZrOCl_2$ hydrate was purchased from Strem Chemicals (Zr content was determined by ICP-AES).

Preparation of $K_2[Zr_2(dhpta)_2] \cdot 5H_2O$ ($2 \cdot 5H_2O$). $ZrOCl_2$ hydrate (1.820 g, 5 mmol) in 50 mL H_2O was added slowly into a solution of H_5dhpta (1.611 g, 5 mmol in 500 mL of H_2O containing KOH (0.842 g, 15 mmol)) with stirring at ambient temperature. Evaporation of water from the solution under reduced pressure afforded colorless crystals, which were recrystallized from water. Yield: 61% (1.503 g). Anal. Calcd for $C_{22}H_{26}K_2N_4O_{18}Zr_2 \cdot 5H_2O$: C, 26.81; H, 3.69; N, 5.69; Zr, 18.52. Found: C, 26.78; H, 3.51; N, 5.30; Zr, 18.54. Crystals suitable for X-ray diffraction were obtained by slow evaporation of a 30 mM aqueous solution of **2** at pH 3.3, 277 K.

The pH of a sample of **2** in H_2O (60 mM) was adjusted to 12 with 0.2 M KOH and then left to crystallize at 277 K. X-ray diffraction showed that crystals obtained at pH 12 had the same structure as those obtained at pH 3.3.

Preparation of $Na_2[Zr_2(dhpta)_2] \cdot 4H_2O$ ($3 \cdot 4H_2O$). $ZrOCl_2$ hydrate (1.820 g, 5 mmol) in 50 mL of H_2O was added slowly into a solution of H_5dhpta (1.611 g, 5 mmol) in 500 mL of H_2O containing NaOH (0.4 g, 10 mmol) with stirring at ambient temperature. Evaporation of water from the solution under reduced pressure afforded colorless crystals, which were recrystallized from water. Anal. Calcd for $C_{22}H_{26}N_4Na_2O_{18}Zr_2 \cdot 4H_2O$: C, 28.26; H, 3.67; N, 5.99; Zr, 19.51. Found: C, 28.49; H, 3.34; N, 5.88; Zr, 20.21. Crystals suitable for X-ray crystallography were obtained as $Na_2[Zr_2(dhpta)_2] \cdot 7H_2O \cdot (CH_3CH_2OH)$ from a solution in H_2O containing a small amount of ethanol after 3 days at 277 K.

Preparation of $Cs_2[Zr_2(dhpta)_2] \cdot 2H_2O \cdot HCl$ ($4 \cdot 2H_2O \cdot HCl$). $ZrOCl_2$ hydrate (1.820 g, 5 mmol) in 50 mL of H_2O was added slowly into a solution of H_5dhpta (1.611 g, 5 mmol) in 500 mL of H_2O containing $CsOH \cdot H_2O$ (2.56 g, 15 mmol)) with stirring at ambient temperature. Evaporation of water from the solution under reduced pressure afforded colorless crystals, which were recrystallized from water. Anal. Calcd for $C_{22}H_{26}Cs_2N_4O_{18}Zr_2 \cdot 2H_2O \cdot HCl$: C% 22.87, H% 2.62, N% 4.85, Zr% 15.79. Found: C% 22.14, H% 3.03, N% 5.17, Zr 17.50%. Crystals suitable for X-ray crystallography were obtained as $Cs_2[Zr_2(dhpta)_2] \cdot H_5O_2 \cdot Cl \cdot 4H_2O$ from an aqueous solution after 3 days at 277 K.

X-ray Crystallography. Diffraction data for **2**−**4** were collected with Mo Kα radiation on a Bruker Smart Apex CCD diffractometer equipped with an Oxford Cryosystems low-temperature device. Absorption corrections were carried out using the program SADABS. Structures were solved by direct methods (SHELXTL or SIR92). All structures were refined against F^2 using all data (SHELXTL). H-atoms attached to water molecules were either located in Δ*F*-maps and refined, or were not placed at all; all other H-atoms were placed in calculated positions and allowed to ride on their parent atoms. In complex **2**, one $K-OH_2$ moiety is disordered over two sites; the relative occupancies were refined. A similar feature was observed in **3**, where in addition there is a further disordered molecule of ethanol. The cesium complex, **4**, is fully

(9) (a) Harding, M. M.; Mokdsi, G. *Curr. Med. Chem.* **2000**, *7*, 1289−1303. (b) Ghosh, P.; D'Cruz, O. J.; Narla, R. K.; Uckun, F. M. *Clin. Cancer Res.* **2000**, *6*, 1536−1545.
(10) (a) Zhong, W. Q.; Parkinson, J. A.; Guo, M. L.; Sadler, P. J. *J. Biol. Inorg. Chem.* **2002**, *7*, 589−599. (b) Alexeev, D.; Zhu, H. Z.; Guo, M. L.; Zhong, W. Q.; Hunter, D. J. B.; Yang, W. P.; Campopiano, D. J.; Sadler, P. J. *Nat. Struct. Biol.* **2003**, *10*, 297−302.
(11) (a) Clearfield, A.; Vaughan, P. A. *Acta Crystallogr.* **1956**, *9*, 555−558. (b) Mark, T. C. W. *Can. J. Chem.* **1968**, *46*, 3491−3497. (c) Aberg, M. *Acta Chem. Scand.* **1977**, *A31*, 171−181.
(12) Veyland, A.; Dupont, L.; Pierrard, J.-C.; Rimbault, J.; Aplincourt, M. *Eur. J. Inorg. Chem.* **1998**, *11*, 1765−1770.
(13) Hoard, J. L.; Silverton, E. W.; Silverton, J. V. *J. Am. Chem. Soc.* **1968**, *90*, 2300−2308.
(14) Held, P.; Listl, B.; Tillmanns, E.; Ahrweiler, A.; Hellwig, H.; Bohaty, L. *Z. Kristallogr.* **2000**, *215*, 65−71.
(15) (a) Pozhidaev, A. I.; Porai-Koshits, M. A.; Polynava, T. N. *Zh. Strukt. Khim.* **1974**, *15*, 644−645. (b) Haussuhl, E.; Gramlich, V. *Z. Kristallogr.* **2000**, *215*, 375−376. (c) Mistryukov, V. E.; Sergeev, A. V.; Mikhailov, Y. N.; Shchelokov, R. N.; Chuklanova, E. B. *Zh. Neorg. Khim.* **1995**, *40*, 1651−1654.
(16) (a) Jameson, D. L.; Xie, C.-L.; Hendrickson, D. N.; Potenza, J. A.; Schugar, H. J. *J. Am. Chem. Soc.* **1987**, *109*, 740−746. (b) Kato, M.; Yamada, Y.; Inagaki, T.; Mori, W.; Sakai, K.; Tsubomura, T.; Sato, M.; Yano, S. *Inorg. Chem.* **1995**, *34*, 2645−2651. (c) Tanase, T.; Inagaki, T.; Yamada, Y.; Kato, M.; Ota, E.; Yamazaki, M.; Sato, M.; Mori, W.; Yamaguchi, K.; Mikuriya, M.; Takahashi, M.; Takeda, M.; Kinoshita, I.; Yano, S. *J. Chem. Soc., Dalton. Trans.* **1998**, 713−718.
(17) (a) Robles, J. C.; Matsuzaka, Y.; Inomata, S.; Shimoi, M.; Mori, W.; Ogino, H. *Inorg. Chem.* **1993**, *32*, 13−17. (b) Gorun, S. M.; Stibrany, R. T.; Lillo, A. *Inorg. Chem.* **1998**, *37*, 836−837. (c) Tanase, T.; Yamada, Y.; Tanaka, K.; Miyazu, T.; Kato, M.; Lee, K.; Sugihara, Y.; Mori, W.; Ichimura, A.; Kinoshita, I.; Yamamoto, Y.; Haga, M.; Sasaki, Y.; Yano, S. *Inorg. Chem.* **1996**, *35*, 6230−6239.

ordered. In the early stages of refinement there appeared to be a problem of charge balance, with the crystal having a formula $Cs_2[Zr_2(dhpta)_2Cl]\cdot 6H_2O$. Careful examination of an electron density difference map, however, showed that two water molecules comprised an $[H_5O_2]^+$ cation.

NMR Spectroscopy. ^1H and $^{13}C\{^1H\}$ NMR data were typically acquired at 298 K and 500 MHz (^1H) using a Bruker DMX500 NMR spectrometer with a 5 mm triple resonance TBI [^1H, ^{13}C, X] probehead capable of delivering single-axis, pulsed field-gradients. Samples were usually 0.6 mL solutions of $K_2[Zr_2(dhpta)_2]\cdot 5H_2O$ in D_2O, or in 9:1 H_2O/D_2O (100 mM Zr, pH 3.30).

One-dimensional (1D) ^1H NMR data were typically acquired over a frequency width of 6 kHz with 16 transients into 32 k data points (acquisition time 2.726 s) using a 7.9 μs (50°) pulse. Water suppression was achieved by low power irradiation during a recycle delay of 3 s.

Two-dimensional (2D) homonuclear ^1H DQFCOSY, TOCSY, and NOESY/EXSY NMR data were typically acquired with 2, 8, and 4 transients, respectively, over a frequency width of 1.1 kHz in both ω_1 and ω_2 into 512 data points for each of 256 t_1 increments with solvent suppression achieved by presaturation during a 2.5 s recycle delay.

2D [^1H,^{13}C] HSQC NMR data were acquired using a gradient-selected, sensitivity-enhanced pulse program.[18,19] The sequence was optimized for $^1J(^1H,^{13}C) = 136$ Hz. Data were acquired over a ^1H frequency width of 1.1 kHz into 512 data points (acquisition time 0.2327 s) with 16 transients for each of 128 t_1 increments over a ^{13}C frequency width of 3.8 kHz centered at 70 ppm using a relaxation delay of 2.5 s between transients. The GARP-1 sequence[20] was used to decouple ^{13}C during data acquisition. The total experiment time was ca. 1.5 h.

2D heteronuclear [^1H, ^{13}C] HMBC NMR data were also acquired using gradient selection and optimized for long range $^1H/^{13}C$ couplings of ~8 Hz ($1/^nJ_{CH} = 60$ ms). Data were acquired over a ^1H frequency width of 1.1 kHz into 512 data points (acquisition time = 0.2327 s) with 32 transients for each of 256 t_1 increments over a ^{13}C frequency width of 16 kHz centered at 125 ppm using a relaxation delay of 2.5 s between transients to give a total experiment time of ca. 6.5 h.

1D $^{13}C\{^1H\}$ NMR data were typically acquired with 1 k transients over a frequency width of 25 kHz into 16384 data points (acquisition time = 0.3269 s) using a 90° pulse and 0.7 s recycle delay. Chemical shifts were referenced internally to the singlet resonance of sodium trimethylsilyl-d_4-propionate (TSP) at 0 ppm and to $NaH[^{13}C]O_3$ at 163.41 ppm in a sealed capillary tube. All data were processed on a Silicon Graphics workstation using XWINNMR (Version 2.0, Bruker).

Potentiometric pH Titration. $K_2[Zr_2(dhpta)_2]\cdot 5H_2O$, **2**, (56.78 mg, 0.1153 mmol Zr) was dissolved in 20 mL of H_2O which was prebubbled with N_2 under heating for 3 h to expel CO_2 thoroughly. Small amounts of 0.2028 M KOH in CO_2-free H_2O were added with stirring, and pH values were recorded after the reading was stable. The temperature was maintained at 293 K.

pH Measurements. Values of pH were determined using a Corning 240 pH meter equipped with a micro combination electrode (Aldrich), calibrated with buffer solutions (Aldrich) at pH 4, 7, and 10. No correction has been applied for the effect of deuterium on the glass electrode for D_2O solutions, and the pH meter reading for a D_2O solution is given as pH*.

ICP-AES. ICP-AES was performed on a Thermo Jarrell Ash IRIS spectrometer using standard methods. The content of Zr was measured without digestion of the samples using the emission line at 349.62 nm. The concentration of Zr in the samples was ca. 80 μM.

pK_a Determinations. ^1H and ^{13}C NMR pH titration data were fitted to the Henderson−Hasselbalch equation using the program KaleidaGraph (Synergy software, Reading PA) to give the pK_a values listed in the text. A least-squares fit to the potentiometric titration data was carried out with the program Scientist (MicroMath).

Results

X-ray Crystal Structures. X-ray crystallography showed that the colorless crystalline complexes, obtained as K(I), Na(I), and Cs(I) salts by reaction of ligand **1** with $ZrOCl_2$ and corresponding hydroxides of potassium, sodium, and cesium in aqueous solution, have similar dinuclear structures for the complex anion (Figures 1 and S1). The crystal data and selected bond lengths and angles are given in Tables 1 and 2.

In the structure of $K_2[Zr_2(dhpta)_2]\cdot 5H_2O$, **2**$\cdot 5H_2O$, each of the two dhpta ligands in the anion $[Zr_2(dhpta)_2]^{2-}$ binds to two Zr(IV) atoms via bridging alkoxide oxygens, carboxylate oxygens, and amine N atoms, giving rise to 8-coordinate Zr(IV). The Zr(IV) and alkoxide O atoms are not coplanar, torsion angle O5A−Zr1−Zr2−O5B = −12.0°. The alkoxide O atom (O5B) from ligand B is 0.28 Å out of the O5A, Zr1, Zr2 plane. The two Zr(IV) centers are almost equivalent with noncrystallographic mirror symmetry through the two alkoxide O atoms and methyne C atoms (torsion angle C6A−O5A−O5B−C6B = 179.8°). The two ligands have different conformations: that of ligand A is more extended than that of ligand B. The two N atoms from ligand A (N1A and N2A) lie in a plane made up of an alkoxide O atom (O5A) and the two Zr(IV) atoms (torsion angles Zr1−N1A/N2A−O5A−Zr2 = 0.5°/0.6°). The methyne C atom (C6A) also lies in this plane. Only ligand A has carboxylate O atoms (O2A and O8A) trans to the bridging alkoxide O atoms (O5A and O5B). The carboxylate groups centered on C4A and C9A each have one O bound to Zr (Zr1 and Zr2, respectively), while the second O is bound to K(I). In ligand B, the two N atoms (N1B and N2B) and the two Zr(IV) atoms also lie along a plane (torsion angle N1B−Zr1−Zr2−N2B = 178.2°). This plane (N1B−Zr1−Zr2−N2B) crosses the plane of ligand A (N1A−Zr1−Zr2−N2A) at an angle of 135.6(5)°. The Zr···Zr distance is 3.5973(4) Å. Each Zr(IV) shows a distorted dodecahedral geometry with the smallest and largest angles being 66.22(7)° (O5A−Zr1−O5B) and 131.34(7)° (O5A−Zr1−O1B). The Zr(IV)−O(alkoxide) distances (2.1427(19)−2.1794(19) Å, average 2.165 Å) are similar to the Zr(IV)−O(carboxylate) distances (2.1269(19)−2.1682(2) Å, average 2.148 Å). The Zr−N distances are longer, 2.433(2)−2.466(2) Å (average 2.448 Å).

Four of the water molecules in **2** are involved in binding to the two K(I) countercations and hydrogen-bond either to

(18) Kay, L. E.; Keifer, P.; Saarinen, T. *J. Am. Chem. Soc.* **1992**, *114*, 10663−10665.
(19) Schleucher, J.; Schwendinger, M.; Sattler, M.; Schmidt, P.; Schedletzky, O.; Glaser, S. J.; Sørensen, O. W.; Griesinger, C. *J. Biomol. NMR* **1994**, *4*, 301−306.
(20) Shaka, A. J.; Barker, P. B.; Freeman, R. *J. Magn. Reson.* **1985**, *64*, 547−552.

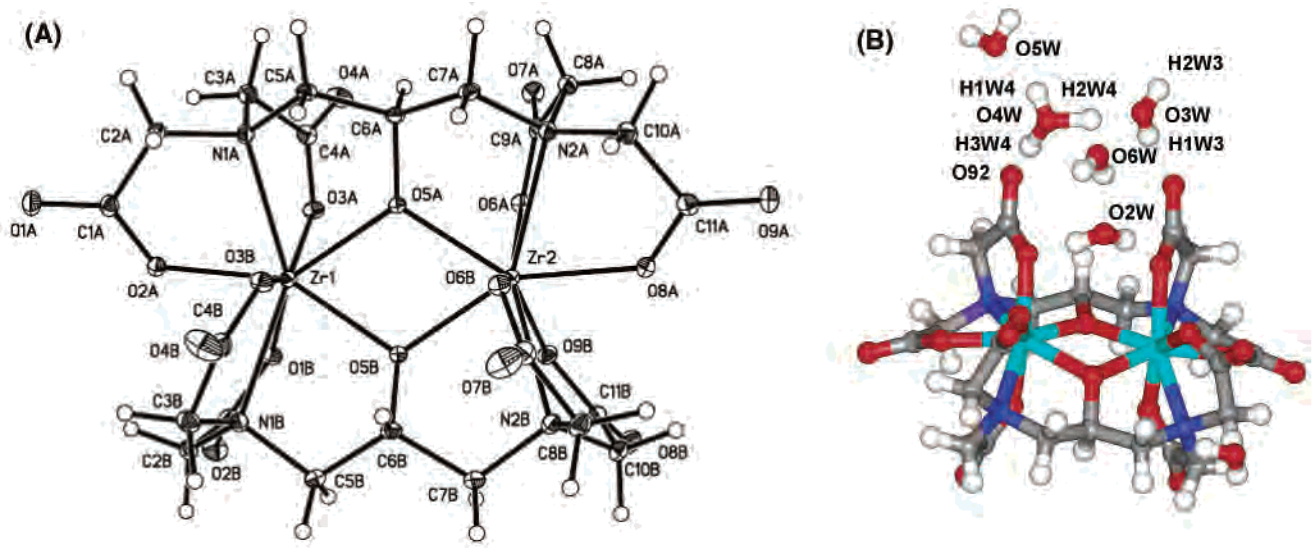

Figure 1. (A) Thermal ellipsoid plot showing the X-ray crystal structure of the dinuclear anion in $K_2[Zr_2(dhpta)_2]\cdot 5H_2O$ (**2**·$5H_2O$) and atom labeling scheme. Ellipsoids enclose 30% probability surfaces. This anion has essentially the same structure in $Na_2[Zr_2(dhpta)_2]\cdot 7H_2O\cdot C_2H_5OH$ (**3**·$7H_2O\cdot C_2H_5OH$) and $Cs_2[Zr_2(dhpta)_2]\cdot H_5O_2\cdot Cl\cdot 4H_2O$ (**4**·$H_5O_2\cdot Cl\cdot 4H_2O$) (see Figure S1). Selected bond lengths and angles are shown in Table 2. Note that the atom labeling schemes differ for the 3 complexes. (B) The H-bond network around the anion in **4**, showing the strong interaction of $[H_5O_2]^+$ with carboxylate oxygen O(92).

Table 1. Crystal Structure Data for Complexes **2**·$5H_2O$, **3**·$7H_2O\cdot C_2H_5OH$, and **4**·$H_5O_2\cdot Cl\cdot 4H_2O$

	complex		
	2·$5H_2O$	**3**·$7H_2O\cdot C_2H_5OH$	**4**·$H_5O_2\cdot Cl\cdot 4H_2O$
formula	$K_2Zr_2C_{22}H_{26}N_4O_{18}\cdot 5H_2O$	$Na_2Zr_2C_{22}H_{26}N_4O_{18}\cdot 7H_2O\cdot C_2H_5OH$	$Cs_2Zr_2C_{22}H_{26}N_4O_{18}\cdot (H_5O_2)\cdot Cl\cdot 4H_2O$
fw	985.19	1035.07	1227.28
color	colorless	colorless	colorless
cryst syst	monoclinic	triclinic	monoclinic
space group	$P2_1/n$	$P\bar{1}$	$P2_1/n$
a (Å)	11.5900(8)	9.4138(12)	14.2765(8)
b (Å)	15.9243(11)	13.9949(18)	13.1465(7)
c (Å)	18.3558(12)	14.9813(19)	20.1326(11)
α (°)	90	75.912(2)	90
β (°)	96.8400(10)	86.104(2)	102.7080(10)
γ (°)	90	73.582(2)	90
V (Å^3)	3363.7(4)	1836.3(4)	3686.0(3)
Z	4	2	4
T (K)	150	150	150
ρ_{calcd} (g·cm^{-3})	1.945	1.872	2.212
μ_{calcd} (mm^{-1})	0.968	0.697	2.682
cryst size/mm^3	0.30 × 0.30 × 0.30	0.33 × 0.25 × 0.12	0.25 × 0.23 × 0.19
F (000)	1992	1056	2392
θ range (deg)	1.70−23.29	1.40−26.42	1.60−26.41
no. reflns collected	20518	15091	20673
no. unique reflns with $I > 2\sigma(I)$	4577	6403	6766
params	505	555	548
R1 ($F_o > 4\sigma(F_o)$)	0.0264	0.0337	0.0374
wR2 (all data)	0.0710[a]	0.0956[b]	0.0772[c]

[a] $w = 1/[\sigma^2(F_o^2) + (0.0376P)^2 + 5.16175P]$, where $P = (F_o^2 + 2F_c^2)/3$. [b] $w = 1/[\sigma^2(F_o^2) + (0.0586P)^2]$, where $P = (F_o^2+2F_c^2)/3$. [c] $w = 1/[\sigma^2(F_o^2) + (0.0265P)^2 + 7.5307P]$, where $P = (F_o^2 + 2F_c^2)/3$.

each other or to a carboxylate O. One of the K(I) ions (K2) is disordered over two sites in the ratio 84:16. The two K(I) ions are 3.922(4) Å apart and are bridged by a carboxylate oxygen (O4A) from ligand A (K−O 2.735(2) and 2.684(2) Å) and by two water molecules O(2W) and O(3WA) (Figure S1, Table S1). One K(I) ion is 8-coordinate while the other is 6-coordinate. The K(I) ions form bridges between three neighboring $[Zr_2(dhpta)_2]^{2-}$ anions.

The sodium salt crystallized as $Na_2[Zr_2(dhpta)_2]\cdot 7H_2O\cdot C_2H_5OH$ (**3**·$7H_2O\cdot C_2H_5OH$), whereas the cesium salt crystallized with an additional proton (and chloride) in the lattice, as $Cs_2(H_5O_2)[Zr_2(dhpta)_2]\cdot Cl\cdot 4H_2O$ (**4**·$H_5O_2\cdot Cl\cdot 4H_2O$). The structure of the anion $[Zr_2(dhpta)_2]^{2-}$ in complexes **3** and **4** is essentially identical to that of complex **2**, showing that the countercations do not affect the basic structure of the dizirconium core (Figure S1). The Zr···Zr interatomic distances are 3.5775(5) and 3.5807(5) Å for complexes **3** and **4**, respectively (Table 2). For complexes **3** and **4**, there are noncrystallographic mirror planes involving the two alkoxide O atoms and methyne C atoms with torsion angles of 179.2°

Table 2. Selected Bond Lengths (Å) and Angles (deg) for Complexes **2**·$5H_2O$, **3**·$7H_2O$·C_2H_5OH, and **4**·H_5O_2·Cl·$4H_2O$

	complex[a]		
	2·$5H_2O$	**3**·$7H_2O$·C_2H_5OH	**4**·H_5O_2·Cl·$4H_2O$
	Bond Lengths[b]		
Zr(1)−Zr(2)	3.5973(4)	3.5775(5)	3.5807(5)
Zr(1)−O(3B)	2.1269(19)	2.1399(18)	2.127(3)
Zr(1)−O(3A)	2.1414(19)	2.1573(18)	2.187(3)
Zr(1)−O(2A)	2.1450(19)	2.1214(19)	2.166(3)
Zr(1)−O(1B)	2.165(2)	2.1618(19)	2.146(3)
Zr(1)−O(5B)	2.1670(19)	2.1771(18)	2.142(3)
Zr(1)−O(5A)	2.1794(19)	2.1419(18)	2.176(3)
Zr(1)−N(1A)	2.435(2)	2.437(2)	2.429(3)
Zr(1)−N(1B)	2.466(2)	2.459(2)	2.454(3)
Zr(2)−O(6B)	2.1347(19)	2.1302(19)	2.169(3)
Zr(2)−O(8A)	2.135(2)	2.136(2)	2.140(3)
Zr(2)−O(5A)	2.1427(19)	2.1582(18)	2.146(3)
Zr(2)−O(9B)	2.167(2)	2.184(2)	2.116(3)
Zr(2)−O(6A)	2.168(2)	2.120(2)	2.202(3)
Zr(2)−O(5B)	2.1714(19)	2.1455(18)	2.172(3)
Zr(2)−N(2A)	2.433(2)	2.442(2)	2.453(3)
Zr(2)−N(2B)	2.457(2)	2.465(2)	2.446(3)
	Bond Angles[b]		
Zr(1)−O(5B)−Zr(2)	112.03(8)	112.60(8)	111.91(12)
Zr(1)−O(5A)−Zr(2)	112.67(8)	111.71(8)	112.20(12)

[a] The labels for atoms refer to complex **2** and the values are entered for the corresponding bonds in complexes **3** and **4** (see Figures 1 and S1). [b] Estimated standard deviations are given in parentheses. See Figures 1 and S1 for atom labels.

and 177.7°, respectively. The two bridging alkoxide O atoms and Zr(IV) atoms also do not lie in a plane, with torsion angles of 11.0° and 12.8° for **3** and **4**, respectively. The anion in **4** is more distorted than in **2** or **3**. The bond lengths Zr−O(alkoxide) are 2.1419(18)−2.1771(18) Å (average 2.156 Å) for **3** and 2.142(3)−2.176(3) Å (average 2.159 Å) for **4**, Zr−O(carboxylate) distances are 2.120(2)−2.184(2) Å (average 2.144 Å) for **3**, and 2.116(3)−2.202(3) Å (average 2.157 Å) for **4**, and Zr−N distances 2.437(2)−2.465(2) Å (average 2.451 Å) for **3** and 2.429(3)−2.454(3) Å (average 2.446 Å) for **4**.

The two Na(I) cations in **3** have distorted octahedral geometry and are bridged by the carboxylate oxygen O92A and by water O5W (Table S1, Figure S1). The Cs(I) ions in **4** are 8- or 9-coordinate and are bridged by carboxyl oxygens O222 and O18B from ligand B (Table S1, Figure S1). A notable feature of this structure, compared to complexes **2** and **3**, is the presence of an additional proton, part of an $[H_5O_2]^+$ unit strongly H-bonded to an oxygen (O92) of a bound carboxylate group (Figure 1B). The H-bond distances O92····H3W4 (1.41 Å) and O3W····H2W4 (1.39 Å) are both short. This structure provides an indication of a possible mechanism for carboxylate dissociation seen in solution.

Solution NMR Data Assignment−Aliphatic Groups. In order to investigate the behavior of complex **2** in aqueous solution, complete assignments were made of its ^1H and ^{13}C NMR resonances. The solid-state structure of the di-Zr(IV) anion displays mirror symmetry along the plane through C6A−O5A−O5B−C6B (Figure 1). If the solution structure resembles the solid-state structure, the symmetry creates pairs of equivalent protons and carbons, thereby halving the anticipated number of NMR resonances. Therefore, 6 carbon and 7 proton NMR resonances would be expected for each ligand in the absence of any fluxional processes. If the two dhpta ligands are inequivalent in solution, as they are in the solid state, a total of 12 carbon resonances (4 of which arise from ^{13}CO) and 14 proton resonances would be observable.

The 500 MHz ^1H NMR spectrum of the K(I) complex **2** in D_2O acquired at 298 K (Figure 2A) consists of 10 resolved signals and an envelope of signals at ca. 3.75 ppm. The $^{13}C\{^1H\}$ NMR spectrum shows 6 aliphatic resonances (Figure 2C) and 4 carbonyl resonances. Two ^1H triplets A ($^1H/^{13}C$ 4.58/77.5) and B ($^1H/^{13}C$ 4.26/76.3), which integrate to one proton each, are assigned to two different methyne protons on two magnetically inequivalent dhpta ligands (see Figure 3 for labels A and B). Five sets of methylene signals are observed for which the protons are magnetically inequivalent, as indicated by the pairs of proton signals associated with single carbon resonances (Figure 2B). The resonances are assigned to geminal pairs of protons in the following way: C/G ($^1H/^{13}C$ 4.00, 3.74/65.2); D/F ($^1H/^{13}C$ 3.91, 3.74/64.3); E/H ($^1H/^{13}C$ 3.81, 3.65/62.5); J/K ($^1H/^{13}C$ 3.40, 3.22/63.1); L/M ($^1H/^{13}C$ 3.08, 2.80/64.2). An additional signal $^1H/^{13}C$ 3.74/65.2 is observed, which has three times the intensity of any of the other signals associated with a methylene pair of protons. One-third of this intensity is from G, the geminal partner of C. Since the molecule contains only methylene and methyne protons (which are accounted for in A and B), the remaining two-thirds of this intensity is accounted for by the presence of two equivalent methylene groups with magnetically equivalent protons G′ and G″. With the exception of this signal and peaks A and B, all other resonances integrate for 2 protons. Additional (boxed) peaks, which appear in Figure 2B, were initially thought to arise from a chemical exchange process. Further insight into this is described shortly.

The ^1H NMR resonances fall broadly into two main types. Resonances C−H, with the exception of G′ and G″, are doublets with large coupling constants (^2J = 16.7 Hz). Resonances A, B, and J−M are either triplets or doublets with smaller coupling constants and arise from the central $CH_2-CH-CH_2$ unit of the dhpta ligand. The relationship between A, B, and J−M was revealed by 2D $^1H-^1H$ DQFCOSY NMR spectroscopy (Figure 2D). The triplet A is coupled to triplet J (intensity 2H), which in turn is coupled to doublet K (intensity 2H). Similarly, triplet B is coupled to triplet M (intensity 2H), which is coupled to doublet L (intensity 2H). The reason for the relationship between these signals, and the rationale behind the observed multiplicities, is as follows.

From the crystal structure of **2** (Figure 1), the following angles can be measured for one dhpta ligand (A):

$$\text{H5AA}-\text{C5A}-\text{C6A}-\text{H6A} = 170.6°$$
$$\text{H7AB}-\text{C7A}-\text{C6A}-\text{H6A} = 174.2°$$
$$\text{H5AB}-\text{C5A}-\text{C6A}-\text{H6A} = 51.1°$$
$$\text{H7AA}-\text{C7A}-\text{C6A}-\text{H6A} = 54.3°$$

If all four protons H7AB, H7AA, H5AB, and H5AA were nonequivalent, H6A would show a maximum multiplicity of 16 lines. This is clearly not the case for the current ^1H

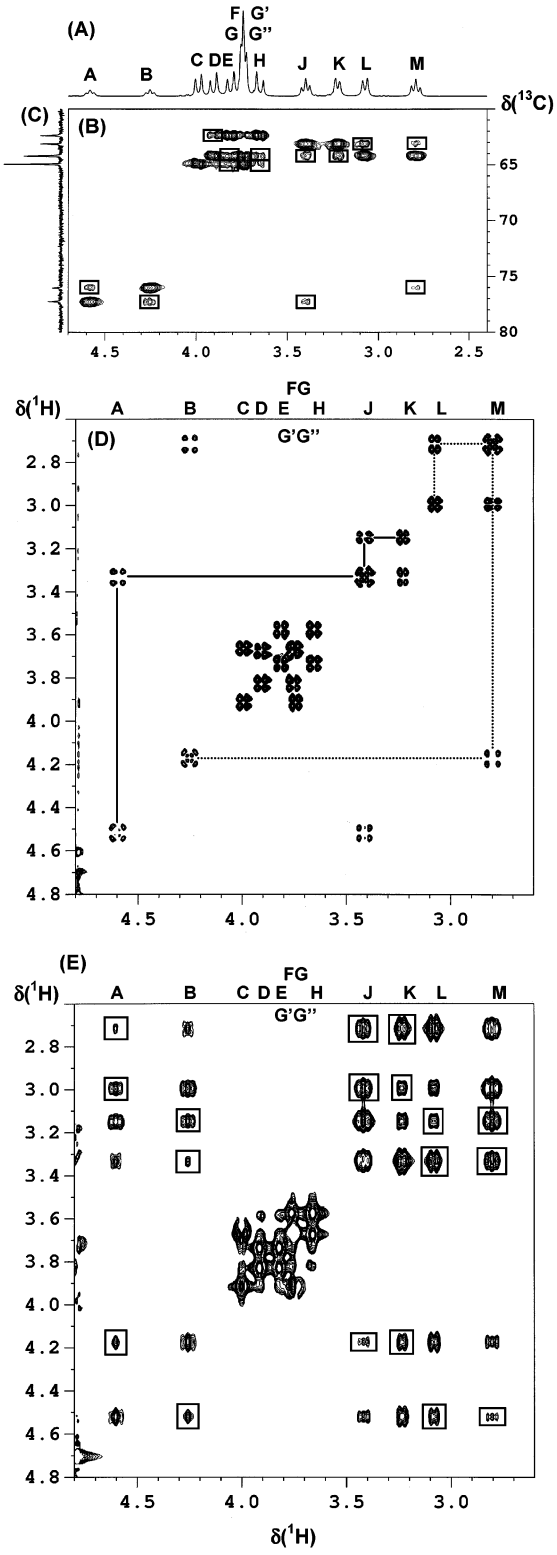

Figure 2. ^{1}H (500 MHz) and ^{13}C (125 MHz) NMR spectra of $K_2[Zr_2(dhpta)_2]\cdot 5H_2O$ (**2**·$5H_2O$) in D_2O at 298 K. (A) ^{1}H NMR spectrum. The peak labels are explained in Figure 3. (B) 2D [^{1}H, ^{13}C] HSQC NMR spectrum showing the presence not only of the expected $^{1}H/^{13}C$ cross-peaks but also of additional peaks (boxed) which are discussed in the text. (C) Aliphatic region of the $^{13}C\{^{1}H\}$ NMR spectrum. (D) 2D $^{1}H-^{1}H$ DQF-COSY NMR spectrum. Connectivities linking the spin systems AJK and BML are indicated by solid and dotted lines, respectively. The absence of DQF−COSY cross-peaks between spin systems AJK and BML and between the methylene resonances C−H is consistent with the presence of 10 isolated spin systems. (E) 2D $^{1}H-^{1}H$ TOCSY NMR spectrum. Inter-spin-system cross-peaks are boxed.

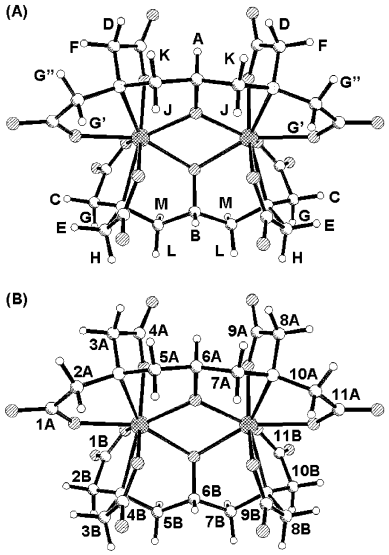

Figure 3. Labeling scheme for atoms of $[Zr_2(dhpta)_2]^{2-}$ used in NMR assignments. (A) Protons and (B) carbons (carbon NMR labels are the same as the crystallographic labels for complex **2**, Figure 1A).

NMR data of the complex. On the basis of previous arguments, it is reasonable to assume that protons H5AB and H7AA are equivalent and that H7AB and H5AA are equivalent, i.e., magnetically equivalent methylene groups. H6A would then appear as a triplet of triplets under these circumstances (i.e., a maximum of 9 lines). However, H6A appears only as a triplet (signal A or B in Figure 2). In a similar way, the simplification of the signals J−M shows an underlying broadening of the NMR resonances. Peak J appears as a triplet due to a large ^{2}J coupling J/K (H5AB−H5AA are a geminal pair) and a large ^{3}J coupling J/A (a torsion angle of ca. 170° results in a large coupling according to the standard Karplus relationship). Peak K appears as a doublet due to the large ^{2}J coupling K/J, but the coupling K/A is less than the resonance line width of K (expected to be ca. 3 Hz based on a torsion angle of ca. 50°). This coupling is therefore unresolved due to resonance broadening.

Similar arguments apply to resonances B, M, and L which are assigned to the second dhpta ligand (B). 2D $^{1}H-^{1}H$ TOCSY NMR data were used to confirm the relationship between A and K and between B and L, the data for which are shown in Figure 2E. However, unlike the 2D COSY NMR data, the TOCSY data revealed a strong correlation between the isolated spin systems AJK and BML (Figure 2E, cross-peaks shown boxed), which represent inter-spin-system correlations. This can be attributed to the presence of a chemical exchange process and explains both the presence of additional cross-peaks in the 2D [^{1}H, ^{13}C] HSQC NMR spectrum and the broadened resonances observed in the 1D ^{1}H NMR spectrum. To investigate this phenomenon fully, and to explain the appearance of the remaining methylene resonances C−H, a series of 2D EXSY NMR data sets was acquired at 298 K with different mixing times. These data sets were used to determine the rate of the chemical exchange process occurring in solution.

A 2D EXSY NMR spectrum at 298 K (mixing time 0.2 s) for complex **2** in aqueous solution is shown in Figure 4

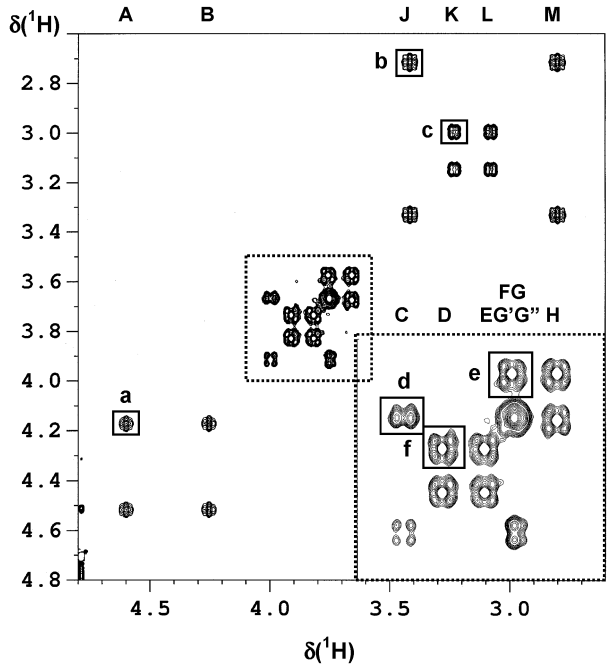

Figure 4. 2D ^{1}H−^{1}H EXSY NMR spectrum of complex **2** in D_2O at 298 K (mixing time 200 ms) showing that protons of $[Zr_2(dhpta)_2]^{2-}$ are involved in chemical exchange processes. Exchange cross-peaks are boxed and labeled a−f, and are rationalized in the text. The dotted box in the bottom right-hand corner shows an expansion of the region for resonances C−H.

with an inset showing the expanded region for the methylene resonances C−H. The absence of TOCSY correlations clarifies the overall behavior of the process. Peaks A and B arise from similar but unique methyne protons from two inequivalent dhpta ligands, A and B. During the process of chemical exchange, ligand A takes on the identity of ligand B and vice versa. Hence, cross-peak a is the result of interconversion between methyne protons A and B from ligands A and B, respectively. Similarly, the two methylene groups J/K interconvert with methylenes L/M leading to cross-peaks b and c (Figure 4).

Methylene ^{1}H NMR resonances C−H also show the same exchange characteristics (Figure 4 inset). Peaks D and E show exchange with one another, and cross-peak f is assigned to D-to-E interconversion. Thus, F and H exchange with one another, and cross-peak e results from F-to-H interconversion since D and F refer to two protons in the same methylene group while E and H are also part of one methylene group (Figure 3), and cross-peak d results from C-to-G′(G″) interconversion.

G′(G″) is a unique singlet resonance in all NMR data sets acquired at pH 3.3 and, as previously described, represents two methylene groups in which all protons and carbons are magnetically equivalent. During pH titration studies (vide infra), it was found that at high pH (11.7) the protons associated with G′/G″ became magnetically inequivalent giving rise to two doublets (G′ and G″) which are coupled to one another.

Determination of Chemical Exchange Rate. In order to determine the exchange rate for the ligand interconversion process in aqueous solution (pH 3.3), 2D EXSY NMR data sets (acquired at mixing times of 10−200 ms at 298 K) were

Table 3. Dependence of Exchange Rate on the Concentration of $K_2[Zr_2(dhpta)_2]\cdot 5H_2O$ (**2**·$5H_2O$) in Aqueous Solution at 298 K

[Zr]/mM	exchange rate[a]/s^{-1}
100	11.4 ± 0.4
50	11.8 ± 0.2
10	11.8 ± 0.4
1	11.6 ± 1.0

[a] Average ±rsd from the EXSY NMR data obtained with mixing times of 10, 30, 50, and 80 ms.

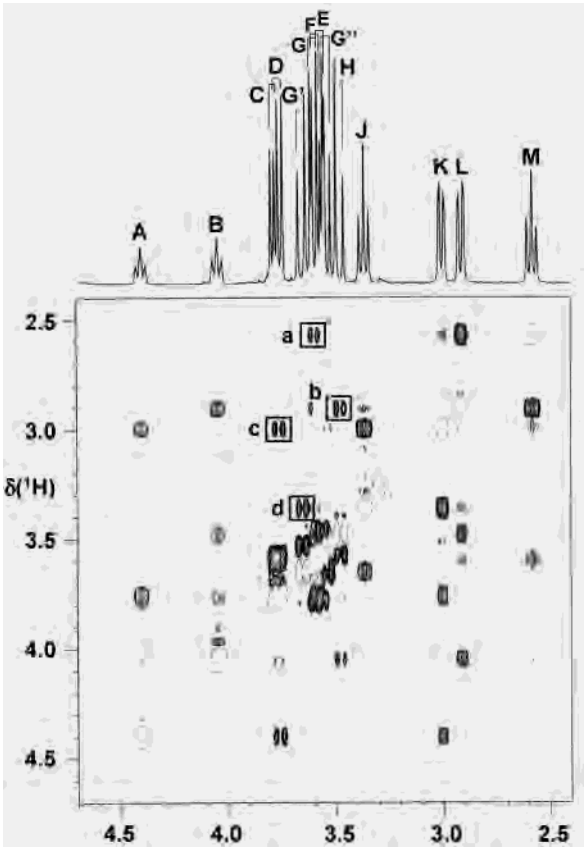

Figure 5. 2D ^{1}H−^{1}H NOESY NMR spectrum for complex **2** at pH 11.7 acquired with a mixing time of 1 s at 298 K. Boxes show nOe's for M/G (a), L/H (b), K/D (c), and J/G′ (d).

quantified by integration. The data were processed using the software package D2DNMR.[21] The exchange rate for the process was found to be 11.4 s^{-1} and independent of Zr concentration over the range 1−100 mM (Table 3).

Assignment of Carboxyl Methylene ^{1}H Resonances. In order to associate carboxyl methylene ^{1}H resonances with specific ligands, through-space nOe correlations were required. Due to the presence of the slow exchange process at pH 3.3, NOESY and related pulse sequences were of no value in providing nOe data. In order to obtain these, it was necessary to arrest the exchange process. This was possible at pH > 10. Figure 5 shows a 2D NOESY NMR data set of the complex at pH 11.7 acquired with a mixing time of 1 s. Although some residual chemical exchange is still apparent (negative cross-peaks), the major part of the data consists of through-space nOes (positive cross-peaks). These relate

(21) Abel, E. W.; Coston, T. P. J.; Orrell, K. G.; Sik, V.; Stephenson, D. *J. Magn. Reson.* **1986**, *70*, 34−53.

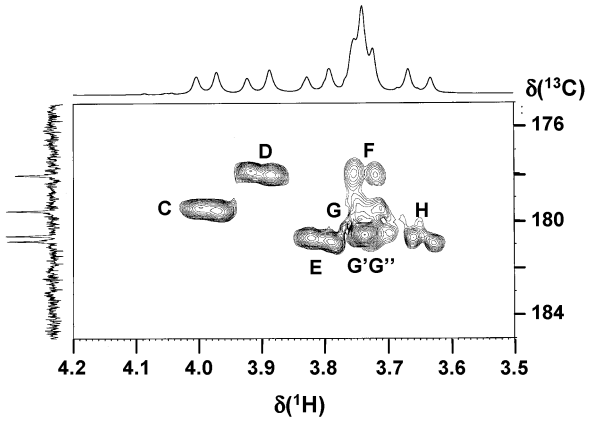

Figure 6. 2D [^{1}H, ^{13}C] HMBC NMR spectrum for complex **2** in D_2O, optimized for 7 Hz long range ^{1}H, ^{13}C couplings. Assignments are shown together with the appropriate region of the 1D ^{1}H (top) and ^{13}C (side) NMR spectra.

proton resonances M/G, L/H, K/D, and J/G′, and enabled a complete assignment of all proton resonances to be made (Figure 3).

Using this information, it was possible to identify the methylene protons and carbons and carbonyl carbons which interchange with one another at pH 3.3. In particular it is clear that proton E (remote from L) interchanges with proton D (which is adjacent to K). This interchange involves rotation of the methylene groups D/F and E/H.

Assignment of Carbonyl ^{13}C Resonances. The binding of carboxyl groups to Zr(IV) would be expected to influence the ^{13}C chemical shift of the associated carbonyl resonance compared with an unbound carboxyl carbonyl. Figure 6 shows an expansion of the carbonyl-to-methylene proton cross-peak region of the 2D [^{1}H, ^{13}C] HMBC NMR data set. Peaks D/F correlate with a ^{13}C carbonyl resonance at 178.0 ppm (carboxylates 4A/9A), C/G with a resonance at 179.5 ppm (carboxylates 1B/11B), and E/H with a resonance at 180.7 ppm (carboxylates 4B/9B). The correlation of G′(G″) is to a carbonyl resonance at 180.5 ppm (carboxylates 1A/11A).

Temperature Dependence. ^{1}H and ^{13}C NMR were used to monitor the temperature-dependent behavior of an aqueous solution of complex **2** in D_2O over the range 298−323 K. As shown in Figure 7, ^{1}H and ^{13}C resonances broadened and decreased in intensity with increase in temperature indicating an increase in the exchange rate at higher temperatures. In the ^{1}H NMR spectrum, the resonances assigned to the methyne protons (A and B) could not be detected at ≥310 K. Resonances K and L coalesced into a broad resonance at 343 K, at which temperature J and M just enter coalescence (underlying broad hump). However, the singlet for G′(G″) remained unchanged.

Resonance broadening with increasing temperature was also observed for ^{13}C{^{1}H} NMR resonances. When the temperature was decreased to 278 K, no significant change was observed in the ^{1}H NMR spectrum, but the ^{13}C resonances sharpened; the resonances corresponding to 2B/10B and 2A/10A (δ^{13}C: 64.9 ppm) and 3A/8A and 5B/7B (δ^{13}C: 64.2 ppm) each split into two sets while resonances 5A/7A and 3B/8B separated from each other. This indicated a slowing down of the ligand interchange process at lower temperatures.

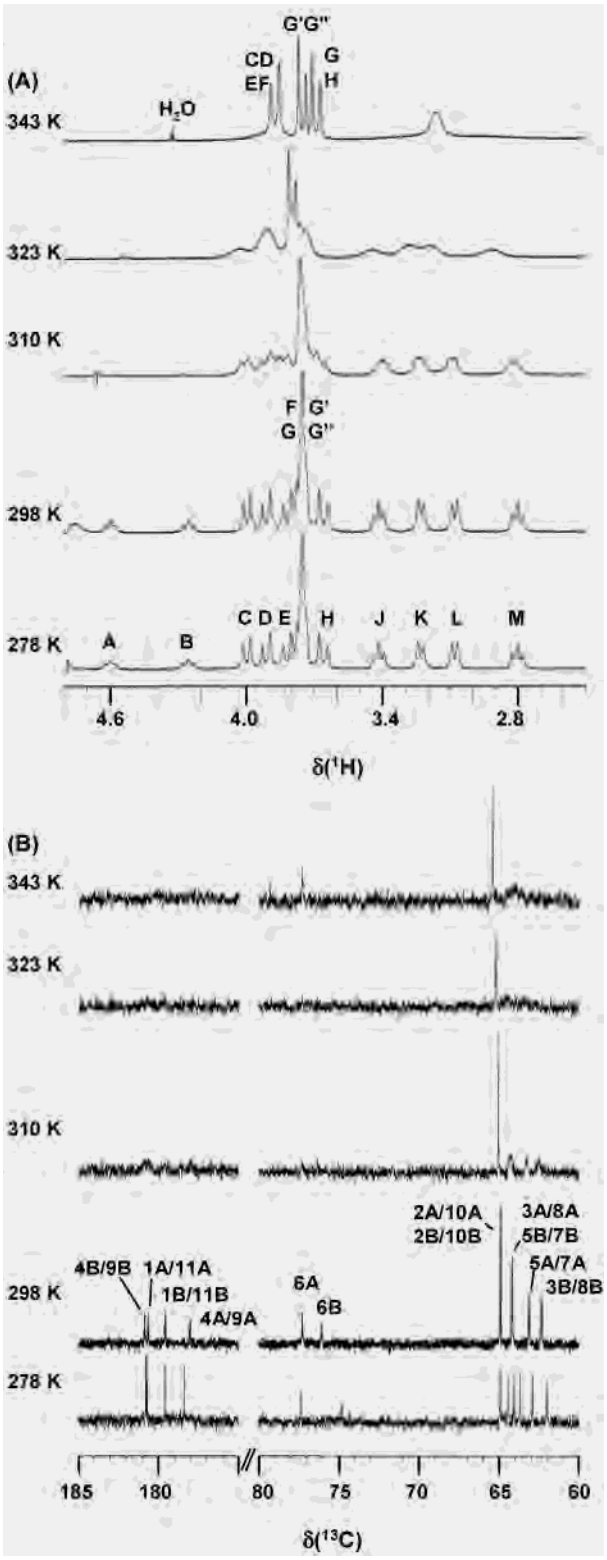

Figure 7. Dependence on temperature of (A) ^{1}H and (B) ^{13}C NMR spectra of complex **2** in D_2O. For labeling scheme, see Figure 3. Chemical-exchange broadening of peaks is evident at higher temperatures.

pH Dependence. The chemical shifts of most of the ^{1}H and ^{13}C NMR resonances of complex **2** were highly dependent on pH over the range ca. 8−12, Figures 9 and S5. The largest ^{1}H shift change was for peak E (−0.25 ppm)

Table 4. Changes in ^{1}H and ^{13}C NMR Chemical Shift of Complex 2 (in ppm) between pH 11.7 and 3.3 (9:1 H_2O/D_2O) at 298 K ($\Delta\delta$ = δ(pH 11.7) − δ(pH 3.3))

	^{1}H (^{13}C)[a]						
	A (6A)	B (6B)	C (2B)	D (3A)	E (3B)	F (3A)	G (2B)
$\Delta\delta(^1H)$	−0.182	−0.206	−0.203	−0.146	−0.250	−0.159	−0.146
$\Delta\delta(^{13}CH)$	−0.104	−4.160	−0.444	−1.180	0.073	−1.180	−0.444
$\Delta\delta(^{13}CO_2)$			1.016	2.105	−0.061	2.105	1.016
	G′ (2A)	G″ (2A)	H (3B)	J (5A)	K (5A)	L (5B)	M (5B)
$\Delta\delta(^1H)$	−0.089	−0.205	−0.175	−0.036	−0.221	−0.162	−0.211
$\Delta\delta(^{13}CH)$	0.572	0.572	0.073	−0.164	−0.164	1.569	1.569
$\Delta\delta(^{13}CO_2)$	1.071	1.071	−0.061				

[a] Labeling scheme is shown in Figure 3.

followed by K (−0.22 ppm) and M (−0.21 ppm), and the smallest was for peak J (−0.04 ppm). The largest ^{13}C shift change was for peak 6B (−4.16 ppm) followed by 2B/10B (+1.57 ppm), and the smallest for peaks 3B/8B (+0.07 ppm) followed by 6A (−0.10 ppm) and 5A/7A (−0.16 ppm). For the carboxylate groups, the largest ^{13}C shift change was for peaks 4A/9A (those connected to protons D/F) (+2.10 ppm), while the smallest was for 4B/9B (those connected to protons E/H) (−0.06 ppm) (Table 4).

With increasing pH, all of the ^{1}H NMR resonances shifted to low frequency by $\Delta\delta$ = 0.1−0.25 ppm, except for resonance J which underwent almost no change in chemical shift (Figures 8A and S5). Resonances F, G, G′, and G″, which overlap below pH 7.75, separated from each other at pH ≥ 8.27. At pH ≥ 10.3, all ^{1}H NMR resonances sharpened, and the G′/G″ singlet separated into two doublets. Moreover, the methyne resonances A and B both appeared as triplets of triplets (in agreement with the expected multiplicities based on the geometry), while resonances K and L appeared as a doublets of doublets (Figure 8B). These results indicate that the exchange process is much slower at high pH.

A computer fit to the ^{13}C shift data gave pK_a values of pK_{a1} = 9.14 ± 0.29 and pK_{a2} = 10.04 ± 0.52 (R = 0.99977). Similar values were obtained from fits to the ^{1}H NMR titration data. The occurrence of two deprotonations for complex **2** between pH 8 and 11 was confirmed by a potentiometric titration, Figure S3, which gave rise to pK_a values of pK_{a1} = 9.02 ± 0.09 and pK_{a2} = 10.02 ± 0.05, in good agreement with the NMR data.

Effect of Ionic Strength. Addition of KNO_3 (0.38−4.5 mol equiv) to an aqueous solution of complex **2** in 9:1 H_2O/D_2O at pH 3.30 did not affect the ^{1}H NMR peaks suggesting that sharpening did not come from the effect of K(I) (data not shown). Considering the changes of resonances G′ and G″, and others as well, the sharpening must be a result of neutralization of the protonated carboxyls or/and hydroxide, which in turn leads to coordination of the deprotonated carboxylates as found in the solid state.

Discussion

Metal complexes of the aminocarboxylate ligand 1,3-diamino-2-hydroxypropane-*N*,*N*,*N*′,*N*′-tetraacetic acid (H_5dhpta) have been studied extensively, especially since it has a strong

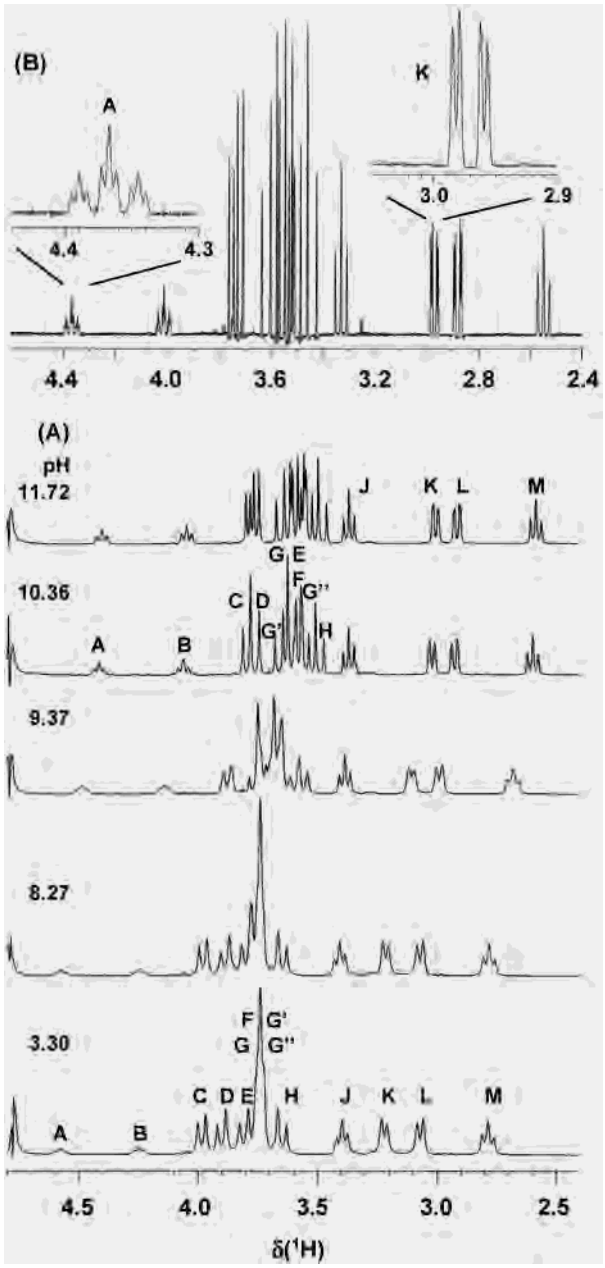

Figure 8. (A) ^{1}H NMR spectra of complex **2** in 9:1 H_2O/D_2O at 298 K at different pH values. (B) Resolution-enhanced spectrum at pH 11.72 with expansions of regions of resonances A and K. For peak labels, see Figure 3.

tendency to give rise to alkoxo-bridged binuclear and tetranuclear species. For Fe(III) and Mn(III), these have served as synthetic models for the active sites of non-heme proteins, and proteins in the oxygen-evolving center of photosystems.[16,17b,22] Dinuclear 2:2 metal/dhpta complexes containing alkoxide bridges are also known for V(III), $[V_2(Hdhpta)_2]^{2-}$ in which V(III) is 7-coordinate and one carboxyl group on each of the two (H)dhpta ligands is protonated and uncoordinated,[17a] and for some lanthanide(III) complexes in which Ln(III) (Ln = Gd, Ho, and Yb) is 8-coordinate.[23] In contrast,

(22) (a) Tanase, T.; Inoue, C.; Ota, E.; Yano, S.; Takahashi, M.; Takeda, M. *Inorg. Chim. Acta* **2000**, *297*, 18−26. (b) Schmitt, W.; Anson, C. E.; Sessoli, R.; van Veen, M.; Powell, A. K. *J. Inorg. Biochem.* **2002**, *91*, 173−189.

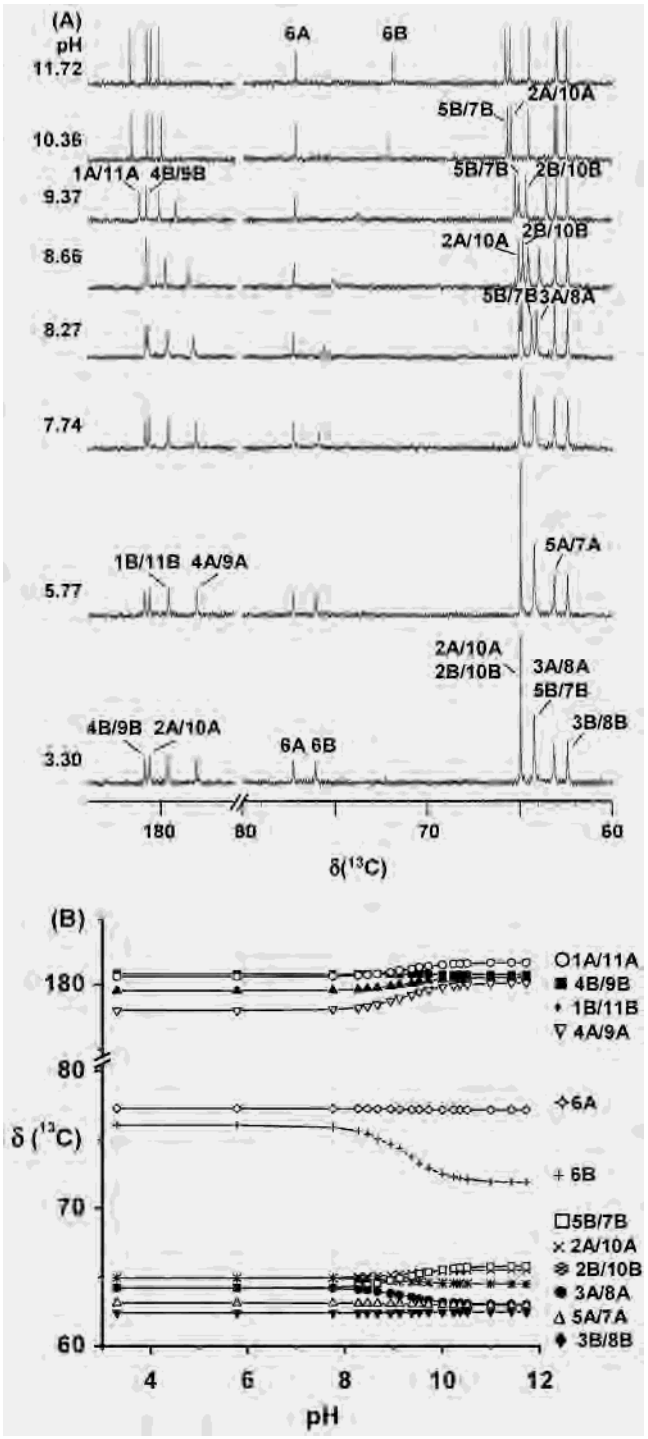

Figure 9. (A) Dependence on pH of the ^{13}C NMR spectrum of complex **2** in 9:1 H_2O/D_2O at 298 K. (B) Plots of ^{13}C NMR chemical shifts versus pH. For peak labels, see Figure 3. The shifts observed between pH 8 and 11 are associated with two deprotonations, and the lines correspond to best fits with pK_a values of 9.14 and 10.04 (see also Figure S4).

Pt(II), Pd(II), and Co(III) can form 1:1 metal/dhpta monomers, in which the 2-hydroxyl group remains protonated and uncoordinated.[24,25]

Solid-State Structures. Our reactions of $ZrOCl_2$ with H_5dhpta in the presence of potassium, sodium, or cesium hydroxides gave metal/dhpta 2:2 dimers with the hydroxyl group deprotonated and acting as a bridge between the Zr(IV) ions, as determined by X-ray crystallography. Fully deprotonated dhpta acts as a heptadentate donor giving 8-coordinate Zr(IV) complexes, similar to those of lanthanide(III).[23] The complex anion $[Zr_2(dhpta)_2]^{2-}$ is essentially identical in complexes **2** (K(I) salt), **3** (Na(I) salt), and **4** (Cs(I) salt). The interatomic Zr···Zr distances of 3.5973(4), 3.5775(5), and 3.5807(5) Å, respectively, are ca. 0.4 Å longer than "typical" Zr−Zr single bonds[26] indicative of little interaction between the Zr(IV) ions in these complexes (ionic radius of 8-coordinate Zr(IV) is 0.98 Å[27]). Zr(IV) adopts a distorted dodecahedral geometry with the largest bond angle of 131.34(7)° and the smallest of 66.22(7)°. In the idealized triangulated dodecahedron $[ZrN_2O_6]$, the angles subtended at Zr(IV) are in the range 69.4−94.3°.[13] The Zr−N average distances in $[Zr_2(dhpta)_2]^{2-}$, 2.448, 2.451, and 2.446 Å, are close to reported values of 2.439 Å for $K_2[Zr(nta)_2]$,[13] 2.471 Å for $(NH_4)_2[Zr(nta)_2]$,[14] and 2.427−2.489 Å for $[Zr(edta)(H_2O)_2]$ and $[Zr(edta)X_2]^{2-}$ ($X = {}^1/_2CO_3^{2-}$ or F^-).[15]

The Zr(IV)−O (alkoxide) distances (2.1419(18)−2.1794(19) Å) are in the expected range for bridging oxygens (Table 2). Such a bridge has been found in many dimer or tetramer complexes of this ligand, for which typical alkoxide−metal distances are the following: O−Mn(II)/Mn(III), 1.942−2.122 Å[17b] (Mn(II) 6-coordinate, ionic radius 0.97 Å, Mn(III) 0.79 Å[27]); O−Fe(III), 1.971−2.066 Å[16] (Fe(III) 6-coordinate, 0.79 Å); O−Ru(III), 1.93−1.95 Å[17c] (Ru(III) 6-coordinate, 0.82 Å); O−V(III), 2.027−2.046 Å[17a] (V(III) 7-coordinate, no ionic radius data available, 6-coordinate 0.78 Å), O−Yb(III), average 2.22(1) Å[23] (Yb(III) 8-coordinate, 1.125 Å). Thus, the Zr−O(alkoxide) bond is slightly longer than analogous reported bonds except those for the large Yb(III) ion. The carboxylate O−Zr(IV) distances of 2.116(3)−2.202(3) Å are close to those in $[Zr(nta)_2]^{2-}$ (2.124−2.251 Å)[13] and $[Zr(edta)X_2]^{2-}$ (2.123−2.179 Å).[15] Of the three structures determined here, complex **4** has the shortest and the longest Zr−O bonds, also indicating that it is more distorted than the other two.

The K−O(carboxylate) (2.684(2)−2.991(2) Å) and K−O(water) (2.709(3)−3.109(5) Å) bond lengths for the 6- and 8-coordinate K(I) countercations in complex **2** are close to those reported for potassium antimony citrate ($K-O_{car}$ = 2.722−2.937 Å and $K-O_{wat}$ = 2.736−2.762 Å) and for potassium copper pyridine-2,6-dicarboxylate hydrate ($K-O_{car}$ = 2.726−2.898 Å and $K-O_{wat}$ = 2.660 − 3.114 Å).[28] Similarly, the Na−O distances for the two 6-coordinate Na(I) ions in complex **3** ($Na-O_{car}$ 2.241(12)−2.717(2) Å, $Na-O_{wat}$ 2.106(8)−2.900(9) Å) are close to those reported for sodium cerium 1,4,7,10-tetraazacyclododecane-tetra-

(23) Miyashita, Y.; Sanada, M.; Yamada, Y.; Fujisawa, K.; Okamoto, K. *Chem. Lett.* **2002**, 840−841.

(24) Kortes, R. A.; Stringfield, T. W.; Ward, M. S.; Lin, F. T.; Shepherd, R. E. *Inorg. Chim. Acta* **2000**, *304*, 60−71.

(25) (a) Sato, M.; Yano, S. *Bull. Chem. Soc. Jpn.* **1989**, *62*, 3932−3938. (b) Yano, S.; Kato, M.; Tsukahara, K.; Sato, M.; Shibahara, T.; Lee, K.; Sugihara, Y.; Iida, M.; Goto, K.; Aoki, S.; Shibahara, Y.; Nakahara, H.; Yanagisawa, S.; Miyagawa, H. *Inorg. Chem.* **1994**, *33*, 5030−5035.

(26) Dekock, R. L.; Peterson, M. A.; Reynolds, L. E. L.; Chen, L. H.; Baerends, E. J.; Vernooijs, P. *Organometallics* **1993**, *12*, 2794−2805.

(27) Shannon, R. D. *Acta Crystallogr.* **1976**, *A32*, 751−767.

acetate hydrate ($Na-O_{car}$ = 2.335−2.389 Å, Na−O(carbonate) 2.927 Å, $Na-O_{wat}$ = 2.342−2.533 Å).[29] The Cs−O bond distances for **4** ($Cs-O_{car}$ 3.029(3)−3.645(3) Å and $Cs-O_{wat}$ 3.086(4)−3.287(4) Å) are similar to those reported for cesium malate hydrate ($Cs-O_{car}$ distances are 3.131−3.307 Å, and $Cs-O_{wat}$ is 3.493 Å).[30] Longer Cs−O distances of up to 3.718 Å have been found in a cesium 18-crown-6 complex.[31] The Cs−Cl distances (3.3834(12) and 3.4174(12) Å) are close to those in a complex of cesium and copper with a calixarene-derivative (3.412−3.526 Å).[32]

Dynamic Exchange in Aqueous Solution. The 2D EXSY data (Table 3) support the conclusion that $[Zr_2(dhpta)_2]^{2-}$ is indeed dinuclear in solution and undergoes a dynamic intramolecular ligand interconversion process with an average lifetime of 88 ms in aqueous solution at pH 3.3, 298 K. The process appears to be mediated by protonation of one carboxylate group on each Zr(IV) ion. This relieves the steric crowding and electrostatic repulsions between the oxygen atoms on the oxygen-rich face of the complex. In the solid state, coordination to alkali metal ions neutralizes the charge on this face, but in solution, there is competition from aquation both of the dinuclear anion and the alkali metal ions. KOH (2 mol equiv per dimer) was needed to sharpen the NMR resonances and arrest the exchange process. At low pH, the methyl protons G′ and G″ have the same chemical shift ($^1H/^{13}C$ 3.741/64.96) but separate from each other at high pH ($^1H/^{13}C$ 3.652, 3.536/65.53), indicating that the acetate group containing protons G′ and G″ (Figure 3) is very flexible. These protons exchange rapidly with each other at low pH on the NMR time scale, but exchange is slowed by deprotonation and coordination at high pH. Curiously though, the only form of the complex which could be crystallized over a wide pH range (despite many attempts) contained only deprotonated carboxylate groups. The two pK_a values determined by potentiometric titration (pK_{a1} = 9.02 ± 0.09, pK_{a2} = 10.02 ± 0.05) agreed well with the values determined from ^{13}C chemical shift data (pK_{a1} = 9.14 ± 0.29, pK_{a2} = 10.04 ± 0.52), Figures S3 and S4). Values of pK_a reported for H_5dhpta itself are 9.49, 7.04, 2.62, and 1.47.[33] Protonation of a carboxylate via H-bonding to $[H_5O_2]^+$ was found in the X-ray crystal structure of the cesium salt complex **4** (Figure 1B). The reported complex $[V_2(dhpta)_2]^{2-}$ contains 7-coordinate V(III) and two protonated uncoordinated carboxyl groups on the (H)dhpta ligands.[17a]

A reasonable assumption is that the ligand exchange process involves protonation of carboxylates 1A/11A of ligand A (Figure 3) so that the carboxylates 1B/11B from ligand B can then occupy the original sites of carboxylates 1A/11A resulting in interconversion of the acetate groups associated with protons E/H, thereby interconverting protons E and D, and H and F, and changing the conformation of ligand A to that of the original conformation of ligand B.

The breaking of the Zr−O bond from each of two carboxyl groups belonging to the same dhpta ligand would result in the following features. First, the dhpta ligands would become magnetically inequivalent, thereby giving rise to two different sets of signals. Second, the methylene protons of the uncoordinated acetate arms would become magnetically equivalent, thereby giving rise to a single set of resonances for both ^1H and ^{13}C. Third, under exchange conditions, the methylene groups that give rise to G′(G″) would bind to Zr through the carboxyl O and would become inequivalent (as at high pH). At the same time, two bound ligands would be released. The overall process would be a "seesaw" effect resulting, in NMR terms, in G′(G″)/C and G′(G″)/G cross-peaks in the EXSY data (Figure 4). All of these features are observed in the NMR data.

The breaking and making of the carboxyl O−Zr bonds can readily be detected on the NMR time scale since the chemical shifts of the relevant carbonyl resonances are all within a 3 ppm range (Table 4). For comparison, the carboxyl ^{13}C resonance of free dhpta (H_5dhpta) undergoes a chemical shift change $\Delta\delta$ of +6.57 ppm from pH 3.37 to 9.13 and of +9.75 ppm from pH 3.30 to 11.19 (2 deprotonations, Figure S2). The exchange process is fast on the NMR time scale: neither unprotonated carboxyls nor protonated carboxyls gave unique resonances, but averaged chemical shifts are observed. The exchange was not affected by the concentration of countercations: no significant changes in either ^1H or ^{13}C NMR chemical shifts were observed on addition of potassium nitrate to solutions of **2**. Opening of Zr−carboxylate chelate rings could be accompanied by coordination of an additional ligand: water/hydroxide. Nine-coordinate Zr(IV) centers have been found in $K_4[Zr(dipic)_3]_2 \cdot 13.5H_2O$ (H_2dipic = 2,6-dicarboxypicolinic acid)[34] and $[Zr(oimda)_2(H_2O)]^{2-}$ (H_3oimda = oxyiminodiacetatic acid).[35]

Conclusions

The structures and dynamics of Zr(IV) aminocarboxylate complexes in aqueous solution are relatively unexplored. Our current interest arises from the possibility of designing Zr-based antibiotics, targeted, for example, to iron uptake systems of pathogenic bacteria. Zr(IV) can compete with Fe(III) for binding to ferrric-ion binding protein (Fbp) from *Neisseria gonnorhoea* and can bind to the tyrosinate oxygens of the dityrosyl motif in the interdomain iron site forming a trinuclear Zr_3 cluster.[36] Zr(IV) also forms strong complexes with human transferrin.[10a] In the current work, we have

(28) (a) Smith, G.; Sagatys, D. S.; Bott, R. C.; Lynch, D. E.; Kennard, C. H. L. *Polyhedron* **1993**, *12*, 1491−1497. (b) Ma, C. B.; Chen, C. N.; Chen, F.; Zhu, H. P.; Liu, Q. T.; Liao, D. Z.; Li, L. C. Cambridge Crystallographic Data Centre Refcode VENDUN01.
(29) Benetollo, F.; Bombieri, G.; Calabi, L.; Aime, S.; Botta, M. *Inorg. Chem.* **2003**, *42*, 148−157.
(30) Fleck, M.; Tillmanns, E.; Bohaty, L. *Z. Kristallogr.* **2001**, *216*, 633−645.
(31) Domasevitch, K. V.; Rusanova, J. A.; Vassilyeva, O. Y.; Kokozay, V. N.; Squattrito, P. J.; Sieler, J.; Raithby, P. R. *J. Chem. Soc., Dalton Trans.* **1999**, 3087−3093.
(32) Xu, W.; Vittal, J. J.; Puddephatt, R. J. *Inorg. Chem.* **1997**, *36*, 86−94.
(33) Powell, J. E.; Ling, D. R.; Tse, P. K. *Inorg. Chem.* **1986**, *25*, 585−586.
(34) Willey, G. R.; Woodman, T. J.; Fisher, M.; Drew, M. G. B. *Transition Met. Chem.* **1998**, *23*, 467−471.
(35) Harben, S. M.; Smith, P. D. Beddoes, R. L.; Collison, D.; Garner, C. D. *Angew. Chem., Int. Ed. Engl.* **1997**, *36*, 1897−1898.
(36) Zhong, W.; Alexeev, D.; Guo, M.; Hunter, D. J. B.; Campopiano, D. J. and Sadler, P. J. 7th International Symposium on Applied Bioinorganic Chemistry, Guanajuato, Mexico, April 1−5, 2003; Abstract p18.

investigated Zr(IV) complexes of the polyaminocarboxylate ligand dhpta which can provide not only amino N and carboxylate O coordination sites but also an alkoxide O.

The bridging role of the alkoxide oxygen was apparent from the X-ray crystal structure of the dinuclear complex $K_2[Zr_2(dhpta)_2]\cdot 5H_2O$. The dinuclear anion $[Zr_2(dhpta)_2]^{2-}$ is highly polarized with one face consisting predominantly of oxygen atoms. In crystals, K(I) ions bind to this oxygen-rich face. In solution, the complex exhibits interesting dynamic behavior, as detected by ^1H and ^{13}C NMR spectroscopy. The two types of coordinated dhpta ligands interconvert on a millisecond time scale at 298 K, illustrating the lability of some of the Zr−O(carboxylate) bonds. An unexpected finding was the pH dependence of the NMR spectra, consistent with two deprotonation reactions with pK_a values of 9.1 and 10.0, and confirmed by potentiometric titration. The X-ray structure did not suggest the presence of deprotonation sites, and even recrystallization at pH 12 gave the same structure for complex **2**.

In order to investigate the potentially special role for the cation in the crystals of **2**, we also determined the X-ray crystal structures of the Na(I) and Cs(I) salts. The dinuclear anion in these complexes (**3** and **4**) has essentially the same structure as that for **2**. The Na(I) and Cs(I) cations also bind to the negative face of the dinuclear anion, although the exact mode of binding differs. In the X-ray structure of the Cs(I) complex **4**, an $[H_5O_2]^+$ unit is strongly H-bonded to a coordinated carboxylate group. The dynamic behavior of the $[Zr_2(dhpta)_2]^{2-}$ anion appears to arise from facile opening of Zr−OCO chelate rings and carboxylate protonation. This may be accompanied by binding of water/hydroxide to Zr(IV). Deprotonation at high pH stabilizes the chelate rings and greatly slows down the chemical exchange process. The high stability of the ring-closed dinuclear structure in the solid state involves alkali metal coordination to the bound carboxylate groups on the oxygen-rich face and leads to isolation of only this form of the complex over a wide pH range. The possibility of achieving high but variable coordination numbers accompanied by pH-controlled ligand exchange proceses is a feature which should be useful in the design of targeted Zr-based therapeutic agents.

Acknowledgment. We thank The Wellcome Trust (Travelling Research Fellowship and International Research Development Award for W.Z.) and the Medical Science Foundation of Chinese PLA (Grant 01H021 for W.Z.) for their support for this project. We acknowledge use of the X-ray crystallographic programs SIR92, SHELXTL, and SADABS (ref 37). We are grateful to Julie Robinson (Medical Illustration, University of Edinburgh) for design of the cover artwork.

Supporting Information Available: Bond lengths and angles for $\mathbf{2}\cdot 5H_2O$, $\mathbf{3}\cdot 7H_2O\cdot C_2H_5OH$, and $\mathbf{4}\cdot H_5O_2\cdot Cl\cdot 4H_2O$ (Table S1; PDF); diagrams showing binding of alkali metal ions to $[Zr_2(dhpta)_2]^{2-}$ in these structures, ^1H and ^{13}C NMR spectra of dhpta at various pH values, potentiometric titration data, and pH dependence of ^{13}C carboxyl NMR resonance of complex **2** (Figures S1−S5; PDF). X-ray crystallographic data are also available in CIF format. This material is available free of charge via the Internet at http://pubs.acs.org.

IC049932K

(37) (a) Altomare, A.; Cascarano, G.; Giacovazzo, C.; Guagliardi, A. SIR92. *J. Appl. Crystallogr.* **1993**, *26*, 343−350. (b) Sheldrick, G. M. *SHELXTL*; University of Göttingen: Göttingen, Germany, 1997. (c) Sheldrick, G. M. *SADABS*; University of Göttingen: Göttingen, Germany, 2001.